

# Different Atmospheric Moisture Divergence Responses to Extreme and Moderate El Niños

Guangzhi Xu · Timothy J. Osborn · Adrian J. Matthews · Manoj M. Joshi

Received: date / Accepted: date

**Abstract** On seasonal and inter-annual time scales, vertically integrated moisture divergence provides a useful measure of the tropical atmospheric hydrological cycle. It reflects the combined dynamical and thermodynamical effects, and is not subject to the limitations that afflict observations of evaporation minus precipitation. An Empirical Orthogonal Function (EOF) analysis of the tropical Pacific moisture divergence fields calculated from the ERA-Interim reanalysis reveals the dominant effects of the El Niño-Southern Oscillation (ENSO) on inter-annual time scales. Two EOFs are necessary to capture the ENSO signature, and regression relationships between their Principal Components and indices of equatorial Pacific sea surface temperature (SST) demonstrate that the transition from strong La Niña through to extreme El Niño events is not a linear one. The largest deviation from linearity is for the strongest El Niños, and we interpret that this arises at least partly because the EOF analysis cannot eas-

ily separate different patterns of responses that are not orthogonal to each other.

To overcome the orthogonality constraints, a Self Organizing Map (SOM) analysis of the same moisture divergence fields was performed. The SOM analysis captures the range of responses to ENSO, including the distinction between the moderate and strong El Niños identified by the EOF analysis. The work demonstrates the potential for the application of SOM to large scale climatic analysis, by virtue of its easier interpretation, relaxation of orthogonality constraints and its versatility for serving as an alternative classification method. Both the EOF and SOM analyses suggest a classification of “moderate” and “extreme” El Niños by their differences in the magnitudes of the hydrological cycle responses, spatial patterns and evolutionary paths. Classification from the moisture divergence point of view shows consistency with results based on other physical variables such as SST.

Guangzhi Xu  
Climatic Research Unit, School of Environmental Sciences,  
University of East Anglia  
E-mail: guang.xu@uea.ac.uk

Timothy J. Osborn  
Climatic Research Unit, School of Environmental Sciences,  
University of East Anglia  
Tel.: +44 (0)1603 592089  
E-mail: T.Osborn@uea.ac.uk

Adrian J. Matthews  
School of Environmental Sciences, University of East Anglia  
Tel.: +44 (0)1603-593733  
E-mail: A.Matthews@uea.ac.uk

Manoj M. Joshi  
Climatic Research Unit, School of Environmental Sciences,  
University of East Anglia  
Tel.: +44 (0)1603 59 3647  
E-mail: M.Joshi@uea.ac.uk

**Keywords** El Niño Southern Oscillation · Self-organizing map · Hydrological cycle

## 1 Introduction

Globally around 60 % of the terrestrial precipitation directly originates from moisture transported from the ocean (Trenberth et al, 2007; Gimeno et al, 2012). The variability of the oceanic water supply greatly influences water availability for all regions. Excessive transports are usually major causes for extreme weather and flood events (Knippertz and Wernli, 2010; Galarneau et al, 2010; Chang et al, 2012; Knippertz et al, 2013), while interrupted transports can lead to droughts and subsequent socioeconomic stresses (Cai et al, 2012, 2014). Hence, a clear understanding of the mechanisms that

force observed changes to the hydrological cycle is of major importance.

Most of the major oceanic source regions of atmospheric moisture are confined to the tropics and subtropics, where the high sea surface temperature (SST) and anticyclonic circulations provide favorable conditions for evaporation to occur under clear sky conditions. The surplus evaporation (E) over precipitation (P) provides a useful estimate of the net water input to the atmosphere (E - P). However, large scale estimates of this flux are largely limited to reanalysis datasets, which suffer from model biases and data inhomogeneity issues (Hegerl et al, 2014; Wang and Dickinson, 2012; Trenberth et al, 2007, 2011). Evaporation from reanalysis is not constrained by precipitation and radiation (Hartmann et al, 2013), spurious trends and biases can be introduced by changing satellite observations (e.g. Bosilovich et al, 2005; Robertson et al, 2011), which also contribute considerably to budget errors over land (Pan et al, 2012). Similarly, precipitation from reanalysis also depends strongly on the parameterization schemes adopted by a specific model (i.e. it is a “type C” variable: Kistler et al, 2001; Kalnay et al, 1996). Moreover, E and P computed oceanic freshwater fluxes show poorer performance in closing the water budget, compared with atmospheric moisture fluxes derived values (Rodríguez et al, 2010).

Therefore, like many studies (e.g. Trenberth and Guillemot, 1998; Trenberth and Stepaniak, 2001) we use the moisture divergence fields computed from “type B” variables (i.e. ones that are more dependent on assimilated observations and less dependent on model parameterizations) to balance the water budget. This indirect approach is more reliable and consistent among observations (Trenberth, 1997b; Roads, 2002, 2003; Gimeno et al, 2012). Moreover, it is the large-scale convergence rather than locally enhanced evaporation that controls the precipitation patterns in the tropics (Mo and Higgins, 1996; Soden, 2000; Su and Neelin, 2002; Trenberth et al, 2003; Zahn and Allan, 2011), and analysis of the moisture divergence provides insights into the major modes of precipitation variability, as well as the moisture sources themselves.

On interannual time scales, large-scale atmospheric variability is closely associated with the El Niño Southern Oscillation (ENSO). Associated with the altered Walker circulation (Bjerknes, 1966, 1969) and strengthened and shifted Hadley cell (Oort and Yienger, 1996; Quan et al, 2004; Hu and Fu, 2007; Wang, 2002) the atmospheric hydrological cycle is also reorganized. Recently, there have been investigations of different types of ENSO events and their corresponding mechanisms and impacts (Capotondi et al, 2014). Most of them

take the SST anomaly (SSTA) patterns as the starting point, and emphasize the different zonal SSTA structures (Larkin and Harrison, 2005a,b; Ashok et al, 2007; Kao and Yu, 2009; Kug et al, 2009; Fu et al, 1986; Trenberth and Stepaniak, 2001; Trenberth and Smith, 2006; Giese and Ray, 2011; Capotondi, 2013). Although each uses a different index definition and separation criterion, and gives different names to the El Niño types and emphasizes somewhat different aspects of these events, it appears that there is some correspondence between these parallel studies:

- the “1972 type ENSO” in Fu et al (1986), the “conventional El Niño” in Larkin and Harrison (2005a) and Ashok et al (2007), the “Eastern Pacific (EP) type ENSO” in Kao and Yu (2009) and Yu and Kao (2007), and the “Cold Tongue (CT) El Niño” in Kug et al (2009), all refer to those events associated with anomalously warm SSTs over the eastern equatorial Pacific;
- the “1963 type ENSO”, the “dateline El Niño” and “El Niño Modoki”, the “Central Pacific (CP) type ENSO”, and the “Warm Pool (WP) El Niño” in the aforementioned studies define the counterpart with its warming centered closer to the central equatorial Pacific.

The events identified by these studies are generally consistent when their data periods overlap (see Fig. 1 in Singh et al (2011) for a summary), suggesting that these diverse interpretations all point to essentially the same phenomena (Kug et al, 2009). Studies starting from spatial patterns in other variables find a similar east-central contrast in the El Niño categorizations: surface salinity (Singh et al, 2011), the first occurrence of significant SSTA (Xu and Chan, 2001; Kao and Yu, 2009), sea level anomalies (Bosc and Delcroix, 2008) and outgoing longwave radiation (OLR) in the equatorial Pacific (Chiodi and Harrison, 2010).

Empirical Orthogonal Function (EOF) analysis is a commonly used technique in studies that describe ENSO. However the orthogonality constraint on the resultant patterns and time-series means that they do not necessarily have direct physical interpretations. This sometimes hampers the ability of this technique to capture non-linear features embedded in the data, particularly when there is a relative spread of variances across multiple EOFs all related to the same forcing. Previous studies suggest that a complete description of different characters and evolutionary features of El Niños cannot be captured fully by a single index, and a second mode reflecting the zonal SST contrast is a necessary complement (Trenberth and Stepaniak, 2001; Trenberth and Smith, 2006; Kao and Yu, 2009). These complemen-

tary modes broadly correspond to the two flavours of El Niños, but have serious deficiencies when considering individual events (Johnson, 2013). In such cases additional efforts and other techniques, like regression analyses, are required to enable a clear interpretation of the EOF results.

Similar to EOF analysis, Self-Organizing Maps (SOM) is a powerful dimension reduction tool, but is free from orthogonality constraint. Introduced into the geography community in the 1990s, it has been more commonly used for determining synoptic circulation patterns and downscaling (Hewitson and Crane, 1994, 2002; Crane and Hewitson, 1998; Reusch et al, 2007; Verdon-Kidd and Kiem, 2009; Verdon-Kidd et al, 2014). Here, we explore its potential applications in large scale climatic analysis. In this study, we first use conventional EOF-correlation analysis to illustrate how the tropical atmospheric moisture circulation responds to different flavours of El Niños. Then, noting that the different types of El Niños are associated with different patterns of anomalous moisture divergence which may not be orthogonal, but EOF analysis imposes orthogonality, we obtain a new perspective from a neural network algorithm (SOM). More details on the SOM algorithm are described in Section 2, including data preprocessing procedures, and the El Niño phase separation method. Sections 3.1, 3.2 and 3.3 show the distinct moisture divergence responses to extreme and moderate El Niños, which is validated by the SOM results described in Section 3.4. A summary and discussion is given in Section 4.

## 2 Methods and Data

### 2.1 Moisture divergence

In this study we use the ERA-Interim (ERA-I) reanalysis data [Dee and Uppala 2009], a third generation atmospheric reanalysis product (Trenberth et al, 2011). ERA-I has some major improvements over its predecessor (ERA-40) in hydrological components (Trenberth et al, 2011), and outperforms NCEP I, II and MERRA in depicting the global ocean-land moisture transports (Trenberth et al, 2011). The near surface fields in ERA-I are better correlated with buoy observations (implying more faithful air-sea water fluxes) compared to NCEP products (Praveen Kumar et al, 2011). And it represents the latest and best reanalysis for reproducing and interpreting the atmospheric branch of the hydrological cycle (Trenberth et al, 2011; Lorenz and Kunstmann, 2012).

Horizontal moisture divergence was computed following Trenberth and Guillemot (1998):

$$\nabla \cdot \mathbf{Q} = \nabla \cdot \frac{1}{g} \int_0^{P_s} q \mathbf{v} dp \quad (1)$$

Specific humidity ( $q$ ), horizontal winds ( $\mathbf{v}$ ) and surface pressure ( $P_s$ ) were obtained from ERA-I for the period of 1st January 1979 to 31st December 2012. Horizontal moisture fluxes were computed on each of the 60 sigma levels using 6-hourly data, to capture as much covariance of  $q$  and  $\mathbf{v}$  as possible. The original full resolution ( $0.75^\circ \times 0.75^\circ$ ) divergence anomaly (with respect to the 34-year mean annual cycle) was temporally averaged into calendar months, and spatially filtered to a lower  $3^\circ \times 3^\circ$  resolution, before passing into the EOF analysis.

### 2.2 ENSO events and phase separation

ERA-I SST data during the same time period were used to compute the Nino 3.4 index (Trenberth, 1997a). After filtering with a 5-month running mean to remove intra-seasonal variability, the time-series was normalized by its standard deviation. El Niño (La Niña) events are determined by the criterion that the Nino 3.4 index exceeds  $+0.75\sigma$  ( $-0.75\sigma$ ) for at least six consecutive months. If this criterion is met, the beginning of the event is defined as the first month that exceeded  $\pm 0.75\sigma$ .

Tracking the evolution of El Niño events through a sequence of phases could be achieved by defining phases according to either their calendar months or their timing relative to the magnitude of the SSTA. Using Nino 3.4 SSTA as the index, Xu and Chan (2001) suggested a 3-month delay in the onset time of “Summer” type El Niños compared with “Spring” type El Niños, which also show distinct warming structures. Considering this time shift in the evolutionary pathways, the calendar-month approach (e.g. using Aug-Oct as the starting phase for both types) might end up comparing events at different evolution stages, particularly for the premature phases.

Therefore, taking into account the irregularity of El Niño events, we defined a relative-amplitude-based method to split each event into five evolutionary phases:

1. “Pre-event” phase: three preceding months before the Nino 3.4 index reaches the El Niño criterion (defined above);
2. “Starting” phase: from the beginning of an event to the time when the Nino 3.4 index rises 70% of the way up to its maximum (See Appendix for an illustration);

- 253 3. “Peak” phase: the phase in between the “Starting” 303  
255 and the “Decaying” phases; 304
- 256 4. “Decaying” phase: from the time when the Nino 3.4 305  
257 index drops 30 % from its maximum value to the El 306  
258 Niño criterion, until the end of the event; 307
- 259 5. the “Post-event” phase: three subsequent months 308  
260 after the Nino 3.4 index drops below the El Niño 309  
261 criterion. 310

262 The Nino 3.4 index experiences fastest changes dur- 312  
263 ing “Starting” and “Decaying” phases (whereby we as- 313  
264 sume swift changes in the overlying atmosphere, which 314  
265 is proved to be the case later). As monthly mean Nino 315  
266 3.4 SST is used, linear interpolation was used to esti- 316  
267 mate the timing of the phases more precisely (i.e. in 317  
268 days). The same interpolating factors are later applied 318  
269 to other variables (e.g. moisture divergence) in creat- 319  
270 ing the phase composites. More details are given in the 320  
271 Appendix. 321

272 Unlike other El Niños that have a single maximum 322  
273 in the Nino 3.4 time-series, the 1986/87 case features a 323  
274 dual peak, with its first peak occurring in January 1987 324  
275 and the second, larger, peak in August 1987. In the 325  
276 phase separation procedure described above, only the 326  
277 second peak was identified as the maximum, and the 327  
278 presence of the first peak was not accounted for. How- 328  
279 ever, computations with the 1986/87 event excluded 329  
280 give very similar results, and suggest that the major 330  
281 conclusions are insensitive to its inclusion. 331

## 282 2.3 Self-organizing maps 332

283 SOM is a type of neural network algorithm that intro- 333  
284 duces a specified number of neurons into the spatio- 334  
285 temporal space of the input dataset, and through an 335  
286 iterative, unsupervised learning process, locates these 336  
287 neurons in such a way that they collectively represent 337  
288 the data values within the entire data space, but in- 338  
289 dividually represent local variability (Kohonen, 1990, 339  
290 2001). Unlike EOF analysis, there are no linear or or- 340  
291 thogonal constraints, and the neuron distribution is de- 341  
292 termined solely by the distribution of the input data. 342  
293 These characteristics allow SOM to represent the di- 343  
294 mensions of the input variables along which the vari- 344  
295 ance in the sequence of inputs is most pronounced (Cava- 345  
296 zos, 1999; Liu et al, 2006). 346

297 In addition to positioning the neurons within the 347  
298 multi-dimensional data space, the neurons are them- 348  
299 selves laid out in a “map” that topologically links them 349  
300 so that neighbouring neurons tend to be more simi- 350  
301 lar than non-neighbouring neurons. This map is most 351  
302 commonly a 2D grid with a hexagonal or rectangular 352

layout that determines how many neighbours each neu-  
ron has (Kohonen, 2001), though other options are pos-  
sible. The topological links between neighbours facili-  
tates examination of evolutionary paths of a physical  
phenomenon across the map’s neurons, as well as effec-  
tively visualizing high-dimensional data and serving as  
an alternative classification method, as will be shown  
in the results section.

Even if it is non-linear, the transition from extreme  
El Niño states to strong La Niña states is nevertheless  
a continuum and we can represent this using SOM with  
a simplified 1D map. Thus, each neuron is topologically  
related only to its immediate neighbours in the 1D ar-  
ray of neurons (of course, each neuron still represents  
a location in the multi-dimensional data space). A de-  
scription of the initialization and training formulation  
to obtain the SOM is given in the Appendix.

The size of the SOM array is usually an arbitrary  
choice made by the user. Analogous to other statistical  
methods, there is a trade-off between the degree of gen-  
eralization, the amount of detail to represent, and the  
capacity of the available data sample to adequately rep-  
resent the variance and distribution of the data. There-  
fore some trial and error experiments are usually rec-  
ommended to determine an appropriate SOM size. In  
this case, a 1D array with five neurons gives results that  
can be easily related to ENSO variability. Using seven  
neurons (not shown) yields similar patterns with large  
differences only occurring in the neutral and moderate  
ENSO states, where the influence of other climate vari-  
ability is relatively larger. This is consistent with John-  
son (2013), who suggested that no more than nine SOM  
neurons could be distinguished in patterns of equatorial  
Pacific SSTA. 336

## 337 3 Results

### 338 3.1 El Niño - La Niña transitions

The two leading EOFs of the moisture divergence anom-  
alies field are found to be ENSO-related, and they ex-  
plain 15 % and 11 % of total variance, respectively. Fig. 1  
displays the patterns and principal components of EOF  
#1 and #2, together with the climatological average  
moisture divergence (negative values indicate moisture  
convergence or  $P > E$ ).

The first EOF (Fig. 1a) features a westward-pointing  
horseshoe structure over the tropical Pacific region that  
is in good agreement with the typical ENSO SSTA pat-  
tern. Anomalous convergence collocates with the warm  
SST anomalies during the mature phase of an El Niño,  
and the encompassing divergent anomalies corresponds  
to the negative SSTAs over the warm pool and South

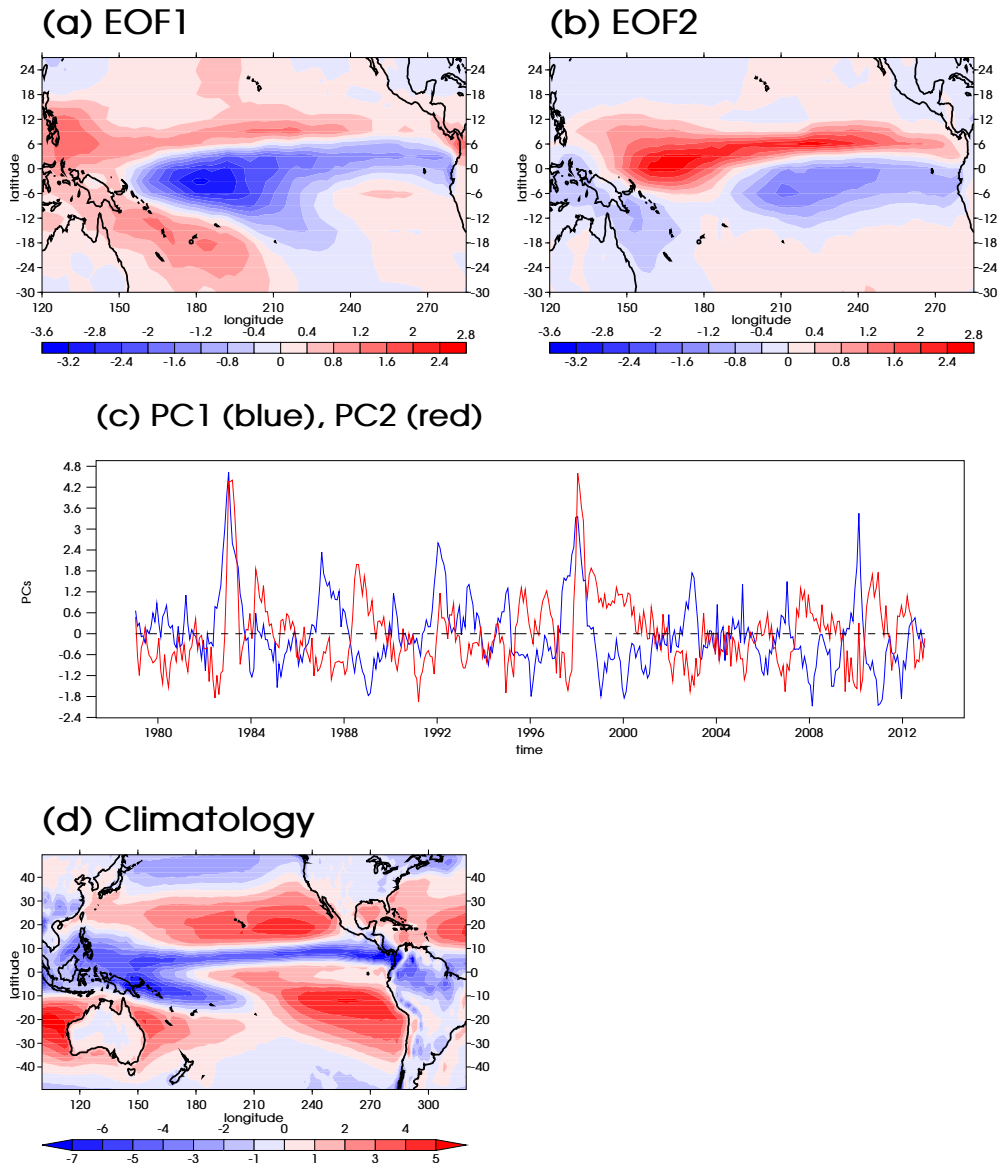


**Fig. 1** Subplots (a) and (b) show the EOF#1 and EOF#2 of tropical Pacific moisture divergence (*mm/day*), respectively. (c) shows their principle component time-series (PC#1 in blue and PC#2 in red). (d) is the climatological mean moisture divergence (1979-2012).

353 Pacific Convergence Zone (SPCZ). This suggests the 365  
 354 influences of thermally driven circulation changes on 366  
 355 the moisture divergence patterns, and the climatologi- 367  
 356 cal convergence/divergence regions (Fig. 1d) are shifted 368  
 357 eastward following the zonal movement of warm SST. 369  
 358 Significant correlations ( $p < 0.01$ ) with Nino 4 ( $r =$  370  
 359 0.68), Nino 3.4 ( $r = 0.85$ ), Nino 3 ( $r = 0.85$ ) and 371  
 360 Nino 1+2 ( $r = 0.70$ ) indices lend further support to 372  
 361 the ENSO attribution. All warm events can be easily 373  
 362 recognized in the PC#1 time-series (Fig. 1c), except 374  
 363 the 1994/95 event (which is also the weakest judging 375  
 364 by the Nino 3.4 amplitude; not shown).

Although this horseshoe-like spatial pattern of EOF#1  
 resembles that in the EOF#2 of Ashok et al (2007),  
 from which they diagnosed the “El Niño Modoki”, the  
 correlation between PC#1 and the El Niño Modoki In-  
 dex is not particularly high ( $r = 0.31, p < 0.01$ ). This  
 is partly due to the different fields used in Ashok et al  
 (2007) (SST) and in this study (moisture divergence),  
 and the non-linear responses of atmospheric circulation  
 to the surface forcing. Therefore this pattern does not  
 effectively distinguish Modoki-associated moisture di-  
 vergence fields from other warm events, but rather rep-  
 resents the broad structure of ENSO cycles in general.

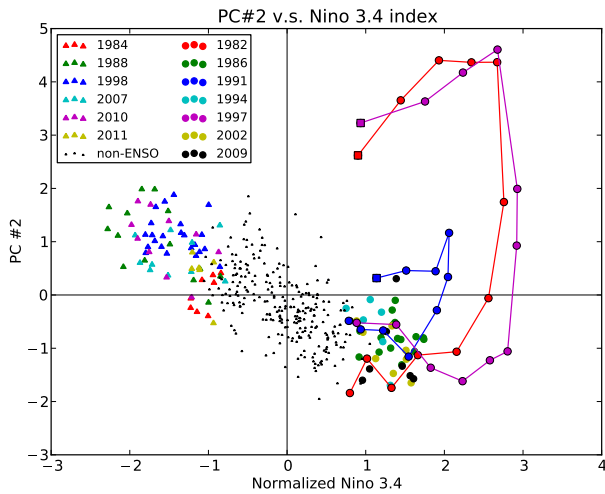


**Fig. 2** Scatter plot of PC#2 against Nino 3.4 index with all El Niño (circles) and La Niña (triangles) events color coded. Non-ENSO months are denoted by small black dots. Evolutionary pathways of the 1982/83 (red), 1991/92 (blue) and 1997/98 (purple) El Niño events are illustrated by solid lines, with the final month being represented with a solid square.

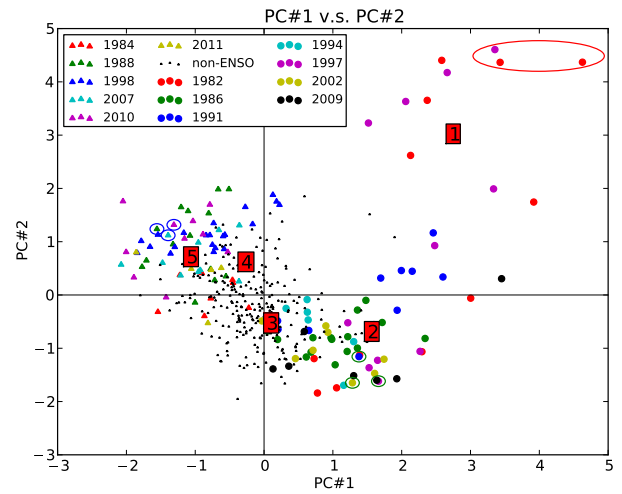


**Fig. 3** Scatter plot of PC#1 and PC#2 with all El Niño (circles) and La Niña (triangles) events color coded. Non-ENSO months are denoted by small black dots. Data points for the extreme El Niño group are enclosed by a red ellipse; the moderate El Niño group by green circles, and the La Niña group by blue circles. Square-boxed numbers show the locations of the five SOM neurons in PC#1, PC#2 space, i.e. regressed onto EOF#1 and EOF#2 using least squares fit.

377 The second EOF pattern (Fig. 1b) features a southwest-  
 378 northeast dipole mode over the western Pacific (west 406  
 379 of the dateline), and a north-south gradient over the 407  
 380 eastern Pacific similar to that found in EOF#1 but 408  
 381 shifted  $6^\circ$  equatorward. The PC#2 time-series (Fig. 1c) 409  
 382 shows more month-to-month variability than PC#1, 410  
 383 but some ENSO signatures are still recognizable, with 411  
 384 the 1982/83 and 1997/98 El Niño cases being most 412  
 385 prominent, similar to the Eastern Pacific index time- 413  
 386 series in Kao and Yu (2009). A closer look at the two 414  
 387 spikes reveals that during these two events they lag 415  
 388 their PC#1 counterparts by about one season, but ex- 416  
 389 perience fast changes, suggesting a quick restructuring 417  
 390 of the moisture circulation patterns. 418

391 Besides greater warming magnitudes, these two warm 419  
 392 events (1982/83 and 1997/98) differ from the others 420  
 393 from a number of additional perspectives (see next sec- 421  
 394 tion). It has previously been noted that two leading 422  
 395 EOFs are required to describe different evolutions of 423  
 396 ENSO events (Trenberth and Stepaniak, 2001; Kao and 424  
 397 Yu, 2009). Therefore we also attribute EOF#2 to ENSO, 425  
 398 representing the non-linear responses not captured by 426  
 399 EOF#1. This non-linearity is illustrated by the outly- 427  
 400 ing dots in the scatter plot of PC#2 against Nino 3.4  
 401 (Fig. 2). In general, PC#2 and Nino 3.4 are negatively 428  
 402 correlated. However, the 1982/83 and 1997/98 events, 429  
 403 and to a lesser extent the 1991/92 case, contaminate 430  
 404 this negative correlation and make the otherwise strong 431  
 405 correlation rather poor ( $r = -0.3, p < 0.01$ ). Not all of 432

the months during these three warm cases are outliers, 433  
 therefore to reveal the evolutionary paths of these ex- 434  
 ceptional events, we linked the points of these events in 435  
 a chronological order. Consistent for all three of them, 436  
 as the El Niño event emerges and rises in amplitude 437  
 (Nino 3.4 increasing), PC#2 decreases, following the 438  
 linear path defined by the negative relationship. When 439  
 Nino 3.4 approaches its maximum value, PC#2 swiftly 440  
 deviates away from the negative relationship and be- 441  
 comes strongly positive. During this period (which will 442  
 be shown to be the peak-to-decaying phases), there is 443  
 no further rise in the SST amplitude, yet the moisture 444  
 divergence field experiences fast changes. Subsequently, 445  
 both Nino 3.4 and PC#2 decrease towards zero. 446

A scatter plot of PC#1 against PC#2 summarizes 447  
 the complete El Niño-La Niña response (Fig. 3). Two 448  
 linear relationships are required to fully capture the 449  
 moisture divergence responses to ENSO effects: 450

1. The negative La Niña-neutral-moderate El Niño cor- 451  
 relation ( $r = -0.46, p < 0.01$ );
2. The positive moderate-extreme El Niño correlation 452  
 ( $r = 0.64, p < 0.01$ );

Although both are statistically significant, these two 453  
 linear relationships represent very different time sub- 454  
 sets (97% and 3% of the data, respectively). Despite 455  
 extreme El Niños only constituting around 3% of the 456  
 total time (14 out of 408 months exceeding  $2\sigma$  in Nino 457

3.4), both PC#1 and PC#2 show high positive values, and the associated reorganization of atmospheric convection and related global disruptions (Cai et al, 2014), mean that special attention to these extreme cases is well deserved.

Three groups of nearby points are circled in Fig. 3 to represent typical patterns for extreme El Niño state (1983-1, 1983-2, 1998-1), moderate El Niño state (1991-11, 1997-8, 2002-11) and strong La Niña state (1988-12, 2007-12, 2010-11), respectively. Other states can be approximated by the linear relationships defined above. The composite for each group was generated by averaging the linear combinations of EOF#1 and #2 from the corresponding months, and the results are shown in Fig. 4. The spatial pattern of the strong La Niña composite (Fig. 4a) is similar to that of EOF#1, and the moderate El Niño composite (Fig. 4c) but with opposite sign. This is a result of both PC#1 and PC#2 switching sign but remaining approximately the same magnitude (Fig. 3). The extreme El Niño group (Fig. 4e) displays distinct spatial patterns and stronger magnitudes (note the different color scale). Both the maximum convergence and divergence in the extreme El Niño composite reach  $13.0 \text{ mm/day}$  or above, which is more than twice the December to February (DJF) climatology (not shown). A zonally elongated convergence band occurs over the eastern Pacific, which co-locates with enhanced precipitation anomalies (Kug et al, 2009; Cai et al, 2012). The climatological SPCZ swings equatorward by a larger amount than during moderate El Niños (the zonal SPCZ feature will be discussed in the next section). A sharp meridional gradient covers the entire tropical Pacific. This is suggested to be the response to the weakened meridional SST contrast over the eastern Pacific (Cai et al, 2014), and the descent anomalies to the north of the equator, mostly caused by dry advection (Su and Neelin, 2002). Lastly, the NH branch of the Hadley cell intensifies in both the ascending and descending branches and shifts equatorward by a larger magnitude (Hu and Fu, 2007; Quan et al, 2004).

These expressions in the space defined by EOFs #1 and #2 of the anomalous moisture divergence during these three event composites are a good representation of the anomaly fields in the full dimensional space (compare Fig. 4a,c,e with Fig. 4b,d,f). This is especially so for the strong La Niña and extreme El Niño composites, while the moderate El Niño composite (Fig. 4d) shows moisture divergence anomaly features in the South Pacific that are not represented by only EOFs #1 and #2 (Fig. 4c). Note that some anomalous features are expected when using a composite formed from only three monthly fields.

### 3.2 El Niño classification

Given the unusualness of the three warm events, it is justified to make the following El Niño classification from a moisture divergence perspective:

1. Extreme El Niño: represented by 1982/83, 1991/92 and 1997/98 cases;
2. Moderate El Niño: represented by 1986/87, 1994/95, 2002/03 and 2009/10 cases.

The 1982/83 and 1997/98 events have been found to be exceptional in various El Niño classification studies, either from an SSTA zonal contrast point of view (Kug et al, 2009; Kao and Yu, 2009; Larkin and Harrison, 2005a,b; Giese and Ray, 2011), or by the SSTA onset timing differences (Xu and Chan, 2001), or using variables other than SST (Singh et al, 2011; Chiodi and Harrison, 2010). The results presented above suggest distinct features from a moisture divergence perspective, and therefore differentiates El Niños on a new dimension.

Unlike the unambiguity in the 1982/83 and 1997/98 cases, the 1991/92 event falls into different groups in different studies: Kug et al (2009) classified it into the “Mix group” (mix of Cold Tongue and Warm Pool El Niño), and in Kao and Yu (2009) and Singh et al (2011) it was grouped into the EP category. Similarly in the case of moisture divergence responses it diverges from the linear transitions between La Niña and moderate El Niños, but not as much as the other two extreme events (Fig. 2).

To examine the relationship between different El Niño responses to the SSTA zonal structure, we also created scatter plots of PC#2 against Nino 4, Nino 3 and Nino 1+2 indices (not shown). The negative correlation among non-El Niño and moderate El Niño points becomes weaker as the index moves from west to east. This suggests better correspondence between the moderate ENSO cycle and central-western Pacific SST variations, while extreme El Niños are more related to the east-west SSTA contrast. Moreover, Kao and Yu (2009) and Capotondi (2013) also found consistent east-west differences in the subsurface temperature structures associated with the two types of El Niños. Zonal SST gradient, ocean heat content propagation and the thermocline feedback are key to explaining the observed differences in the atmospheric circulation, moisture divergence and subsequently precipitation responses.

### 3.3 El Niño phase comparison

To examine the El Niño differences in more detail, each event is broken into five evolutionary phases accord-

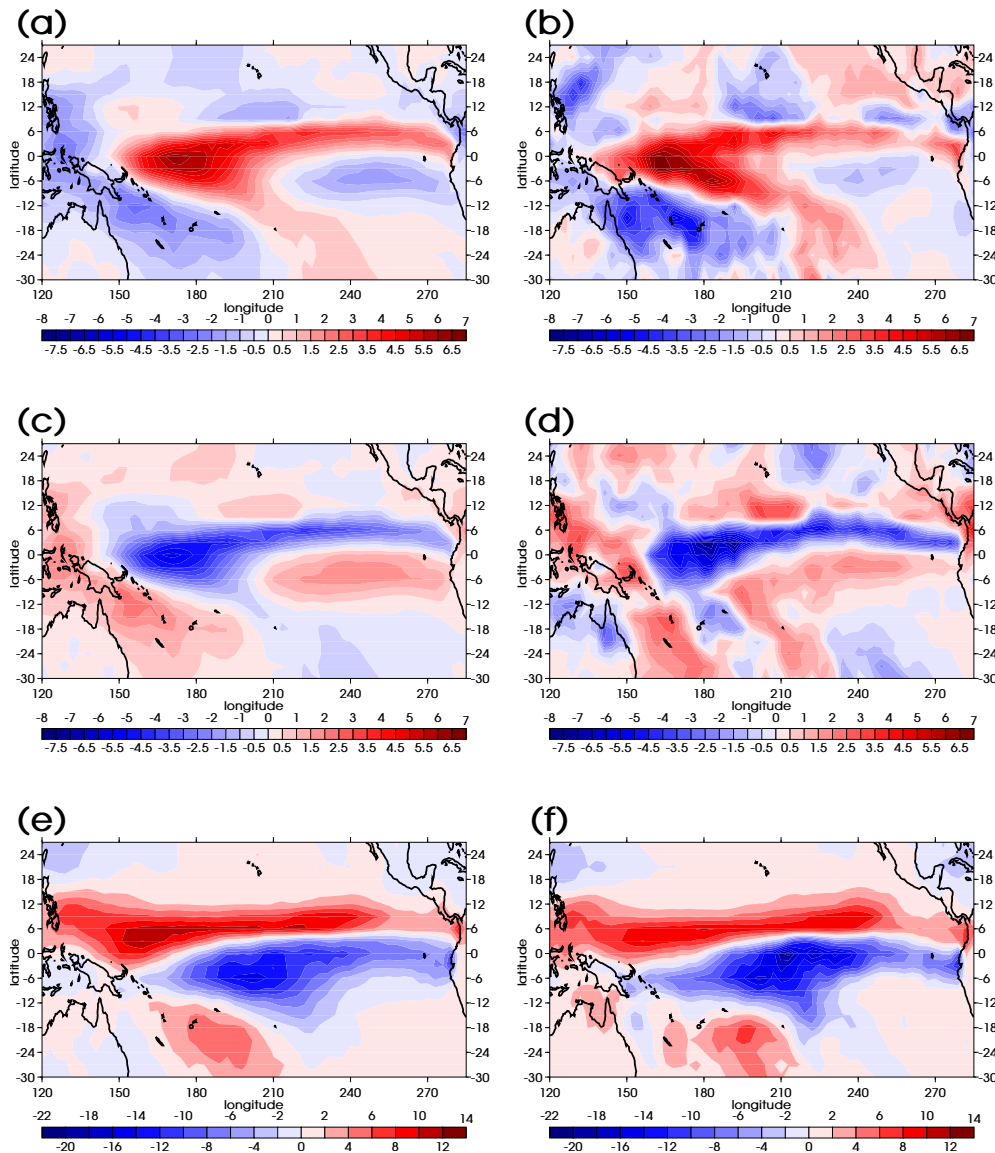


**Fig. 4** Composites of moisture divergence anomaly fields (mm/day) for (a,b) La Niña group. (c,d) moderate El Niño group and (e,f) extreme El Niño group, reconstructed from only EOF#1 and EOF#2 (a,c,e) compared with composites of the actual fields during the same calendar months.

534 ing to their relative Niño 3.4 amplitudes, and the phase 548  
 535 composites for extreme and moderate El Niños are shown 549  
 536 in Fig. 5 and Fig. 6, respectively. 550

537 “Pre-event” and “Post-event” are both 3 months in 551  
 538 duration by definition. With the dual-peaked 1986/87 552  
 539 case excluded, “Starting” phase has an average dura- 553  
 540 tion of 2.9 months, “Peak” phase around 4.0 months 554  
 541 and “Decaying” phase 1.7 months. Therefore an El Niño 555  
 542 would typically experience fast SSTA changes in central 556  
 543 Pacific within one season, then meander for a slightly 557  
 544 longer time in its “Peak” phase, followed by an even 558  
 545 faster drop in SSTA in the “Decaying” phase. 559

546 Although their onset timings and overall durations 560  
 547 differ, the “Peak” phases always occur during the Nov- 561

Dec-Jan season (with the dual-peaked 1986/87 case be-  
 ing exceptional, where the second peak started in July-  
 Aug of 1987). This has been suggested to be the result  
 of a phase-locking mechanism with the seasonal SST cycle  
 (Xu and Chan, 2001; see also Fig. 4 in Wang, 2002),  
 and such a feature would help eliminate the obstacles  
 in inter-comparing the amplitude-based approach and  
 calendar-month-based approach, and promises relation-  
 ships being made with results from other studies.

Notable differences between moisture divergence anoma-  
 lies associated with the extreme and moderate groups  
 start to emerge in the “Starting” phase (Fig. 5 b, 6b),  
 reach a maximum in “Decaying” phase (Fig. 5d, 6d),  
 and persist into the “Post-event” phase (Fig. 5 e, 6e).



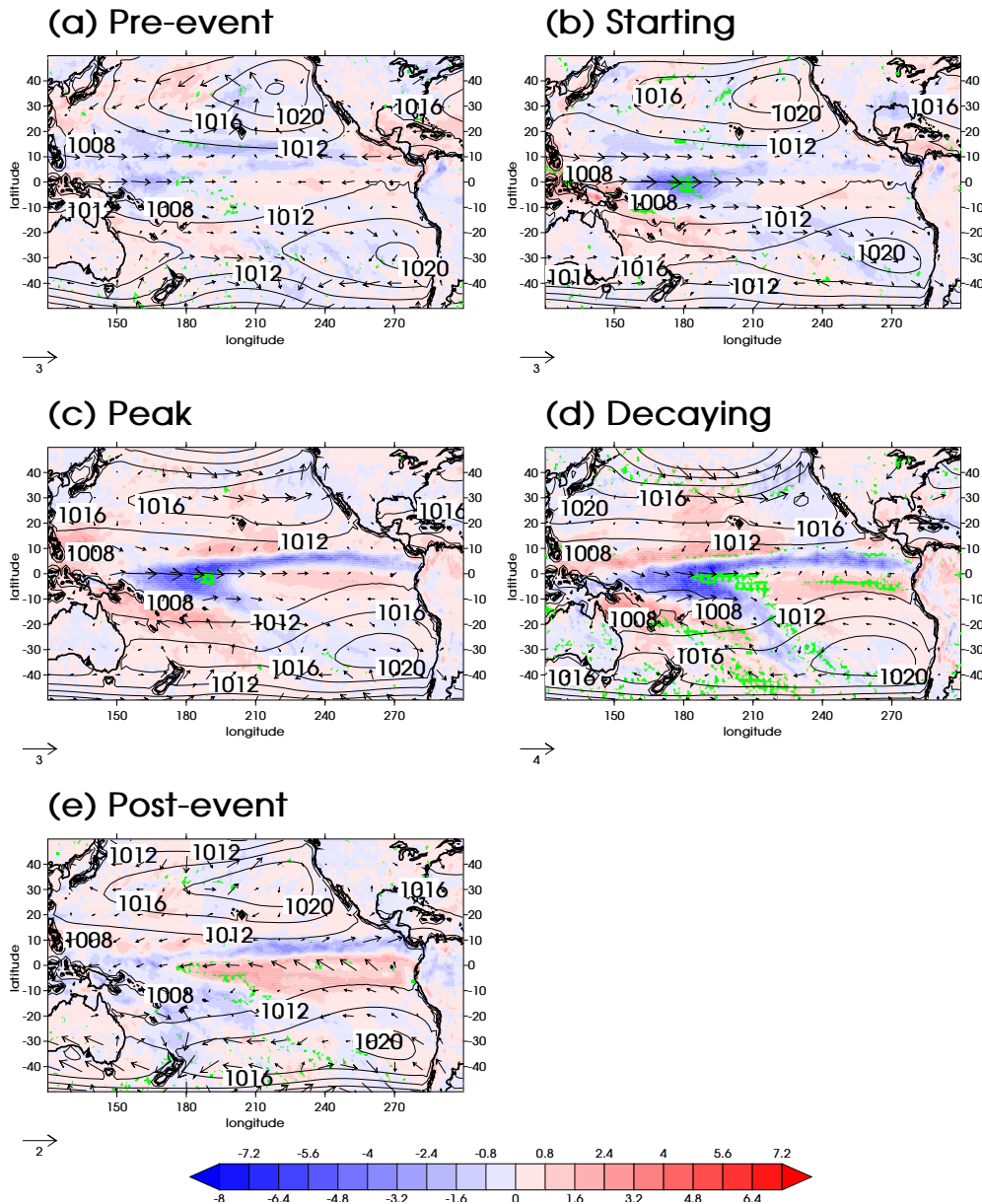


**Fig. 5** Phase composites of moisture divergence anomalies (mm/day) for moderate El Niños in (a) “Pre-event” phase, (b) “Starting” phase, (c) “Peak” phase, and (e) “Post-event” phase. Green hatch overlay denotes areas where the anomaly reverses the sign of the climatology. Surface pressure composite fields are plotted as contour lines with a contour interval of 4 hPa, and 850 hPa horizontal wind anomalies (m/s) are plotted as vectors.

562 In addition to anomalies that are both larger and have 573  
 563 a maximum convergence anomaly further east in the 574  
 564 extreme El Niño composite, an important new finding 575  
 565 is that the extension of the anomalous moisture con- 576  
 566 vergence to the eastern Pacific moves on to the equa- 577  
 567 tor during the peak and decaying phases (Fig. 6c,d), 578  
 568 whereas it stays north of the equator throughout mod- 579  
 569 erate El Niños (Fig. 5). Shoaling of the thermocline 580  
 570 and the resultant influence on SST is very sensitive to 581  
 571 the latitude of the anomalous moisture convergence and 582  
 572 its associated wind stress. This latitudinal difference 583

and the stronger westerly wind anomalies that accom-  
 pany it may contribute to the extension of SSTA fur-  
 ther into the eastern Pacific during extreme El Niños.  
 The anomalous convergence also exists in balance with  
 a more zonally symmetric Southern Hemisphere (SH)  
 surface pressure field and stronger southerlies east of  
 the dateline in the peak and decaying phases, displac-  
 ing the SPCZ to a more zonal orientation (see Cai et al  
 2012).

In contrast, easterly anomalies occur over equatorial  
 eastern Pacific during a moderate El Niño. Together

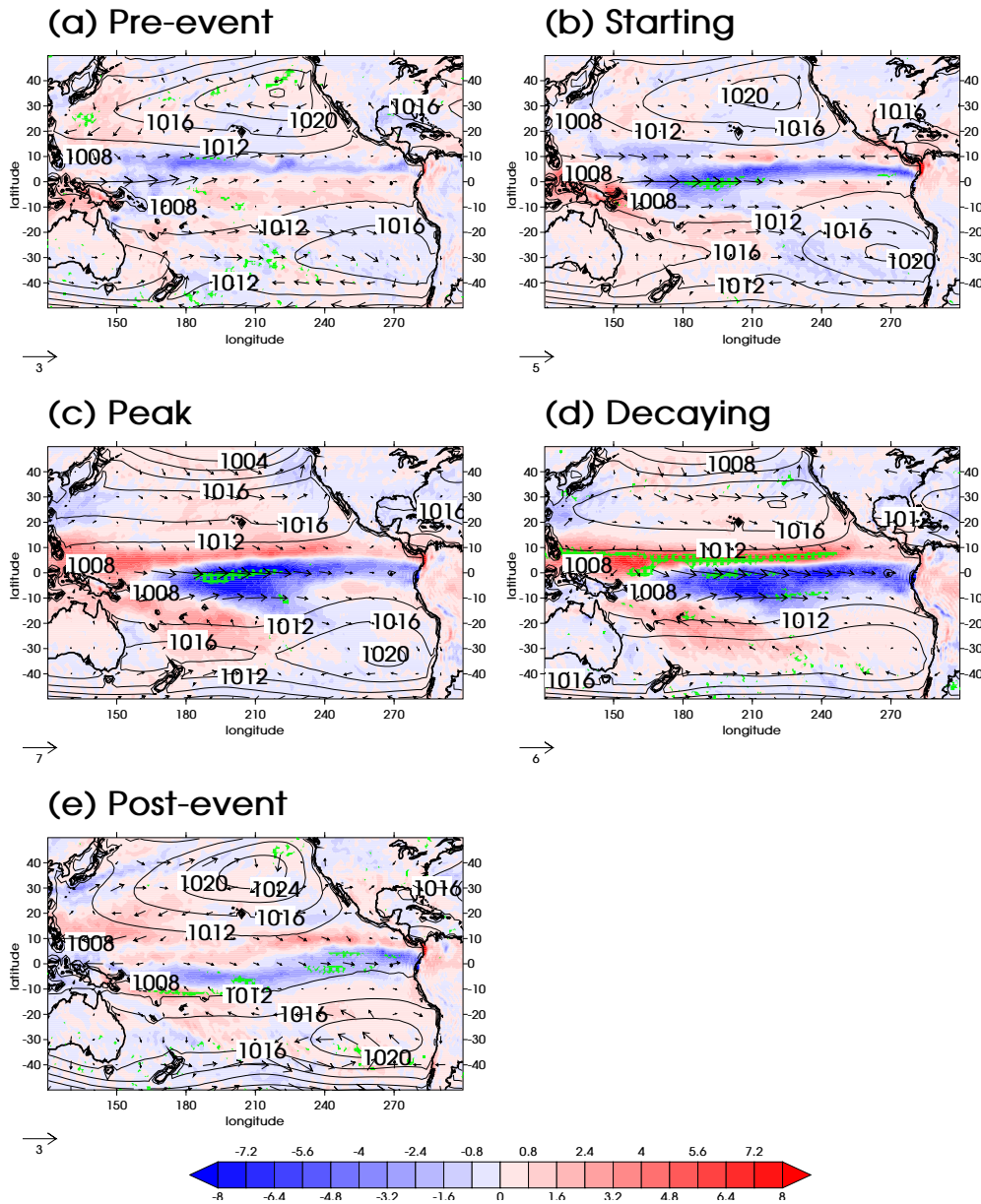


Fig. 6 Same as Fig. 5 but for extreme El Niños.

584 with the off-equator position of the moisture conver- 597  
 585 gence anomaly, these act to confine surface warming 598  
 586 to the central and western Pacific, and deep convection 599  
 587 does not occur in the east (consistent with smaller OLR 600  
 588 reductions, Chiodi and Harrison 2010).

589 To the north of the equator, northwesterly anom- 602  
 590 alies are stronger in the extreme El Niños. Associated 603  
 591 with a more compact NH Hadley cell, this dry advec- 604  
 592 tion helps maintain the sharp meridional gradient in 605  
 593 the moisture divergence field (Su and Neelin, 2002), 606  
 594 which is strong enough to reverse the climatology (in- 607  
 595 dicated by the green hatching in Fig. 6) in the “Decay-  
 596 ing” phase. Moreover, such a peak-to-decaying phase

differentiation is not confined to the moisture diver-  
 gences observed here: the pattern correlations of SSTA  
 from CT El Niños and WP El Niños in corresponding  
 phases (calendar-month-based) were strongly positive  
 during the peak phases of these two types of El Niños,  
 but swiftly become negative one season later (Kug et al,  
 2009). Similar results were also found for precipitation  
 and pressure velocity fields (Kug et al, 2009).

### 3.4 SOM analysis

Although two EOFs capture much of the time-varying  
 ENSO signal, their physical interpretation is hampered

by their lack of independence. Both the EOFs and the PC time-series are constrained, by definition, to be orthogonal, but that does not mean that they are unrelated. This can be seen in Fig. 3, where despite an overall zero correlation between PC#1 and PC#2, a non-linear relationship clearly exists between the two PC time-series. Furthermore, the pattern of EOF#2 will have been constrained so that (a) it is orthogonal to EOF#1; and (b) it has the precise characteristics such that the projection of moisture divergence onto it during the few extreme El Niño months when there is a positive relationship with PC#1 exactly counterbalances the projections during all the other months when there is a negative relationship with PC#1, so that the overall correlation with PC#1 is zero. It is unlikely that EOF#2 will have been unaffected by these constraints, and some ENSO-related information would likely have been spread into higher order EOFs as a result.

This provides the motivation for our SOM analysis of the same moisture divergence field, to explore its utility in easily capturing this non-linear behaviour. By quantifying the distances between a carefully chosen number of SOM neurons, an equivalent El Niño classification is also achieved.

Fig. 7 displays the five SOM neurons we obtained. The 1st neuron (Fig. 7a) shows a good agreement with the extreme El Niño group composite in Fig. 4e, both in terms of spatial patterns and the anomaly strengths. The 2nd (Fig. 7b) and 5th (Fig. 7e) neurons resemble the moderate El Niño group (Fig. 4c) and the La Niña group (Fig. 4a), respectively. Moving from neuron-1 to neuron-5, one observes a gradual transition of the moisture divergence field, therefore the remaining two neurons (neuron-3 and -4) could be expected to represent the neutral and weak La Niña ENSO states.

This attribution is substantiated by the locations of each neuron in the space defined by EOFs #1 and #2, by least squares estimation of the PC#1 and PC#2 coefficients that best replicate each neuron (shown by the red numbered squares in Fig. 3). The sequence of neurons follows the pathway defined by the two correlations. Fig. 8 shows the number of months in each sliding 13-month window allocated to each neuron. The allocation is based upon selecting the closest neuron, in a Euclidean distance sense, to each monthly field. The time-series of neuron-1 displays non-zero values only during the 1982/83 and 1997/98 El Niños, and for a shorter period in the 1991/92 case. The La Niña neuron (neuron-5) shows good correspondence with La Niña years (1983/84, 1988/89, 1999/2000/2001, 2007/08 and 2010/11). Neuron-2 becomes active either during a moderate El Niño (1986/87, 1994/95, 2002/03 and 2009/10) or in the early phase of an extreme El Niño (1982/83

**Table 1** Inter-neuron distances and the means and standard deviations of intra-group distances (mm/day). Distance between neuron  $i$  and  $j$  is denoted by the matrix element at row  $i$ , column  $j$ . The mean and standard deviation of the distances between all training samples and the neuron they are allocated to are listed in the “Mean” and “SD” columns, respectively. Column “Size” shows the size of each group (i.e. number of months).

Neuron	1	2	3	4	5	Mean	SD	Size
1	0	97.6	112.8	105.2	120.6	84.7	7.5	15
2		0	46.1	62.3	81.2	71.4	11.0	50
3			0	31.8	47.6	60.7	7.4	157
4				0	32.4	58.7	7.9	111
5					0	62.6	7.7	75

**Table 2** Correlation matrix between the 5 SOM neurons. Correlation between neuron  $i$  and  $j$  is denoted by the matrix element at row  $i$  and column  $j$ . Note that all correlations are significant at 0.01 level except for the one denoted by asterisk ( $p = 0.33$ ).

Neuron	1	2	3	4	5
1	1	0.34	-0.51	-0.03*	-0.34
2		1	0.29	-0.70	-0.82
3			1	-0.61	-0.48
4				1	0.48
5					1

and 1997/98). The rest of the time period is mostly represented by neutral and weak La Niña neurons (-3 and -4). Instead of the discrete and selection-exclusive sample counting method used here, one could also use a spatially weighted correlation time-series to reveal more subtle features in the temporal variations of each neuron.

To validate the El Niño classifications, we computed inter-neuron distances (Table 1), defined as the Euclidean distance between every two neuron pair, and the mean and standard deviation of intra-group distances. Intra-group distances refer to the distances between all training samples and the neuron they are allocated to. The average and standard deviation of the intra-group distances serve as a measure of how closely the training samples are clustering around the neuron (though note that the distances cannot simply be averaged or summed to represent distances across multiple groups because the distances will be based on different directions in the high dimensional space).

As is shown in Table 1, the extreme El Niño neuron (N1) shows increasingly larger distances from the moderate El Niño (97.6, N2), neutral (112.8, N3), weak La Niña (105.2, N4) and strong La Niña (120.6, N5) neurons. The separation (97.6) between extreme and moderate El Niño neurons is larger than the direct distance from moderate El Niño to strong La Niña (81.2 from N2 to N5). Table 2 shows the pattern correla-

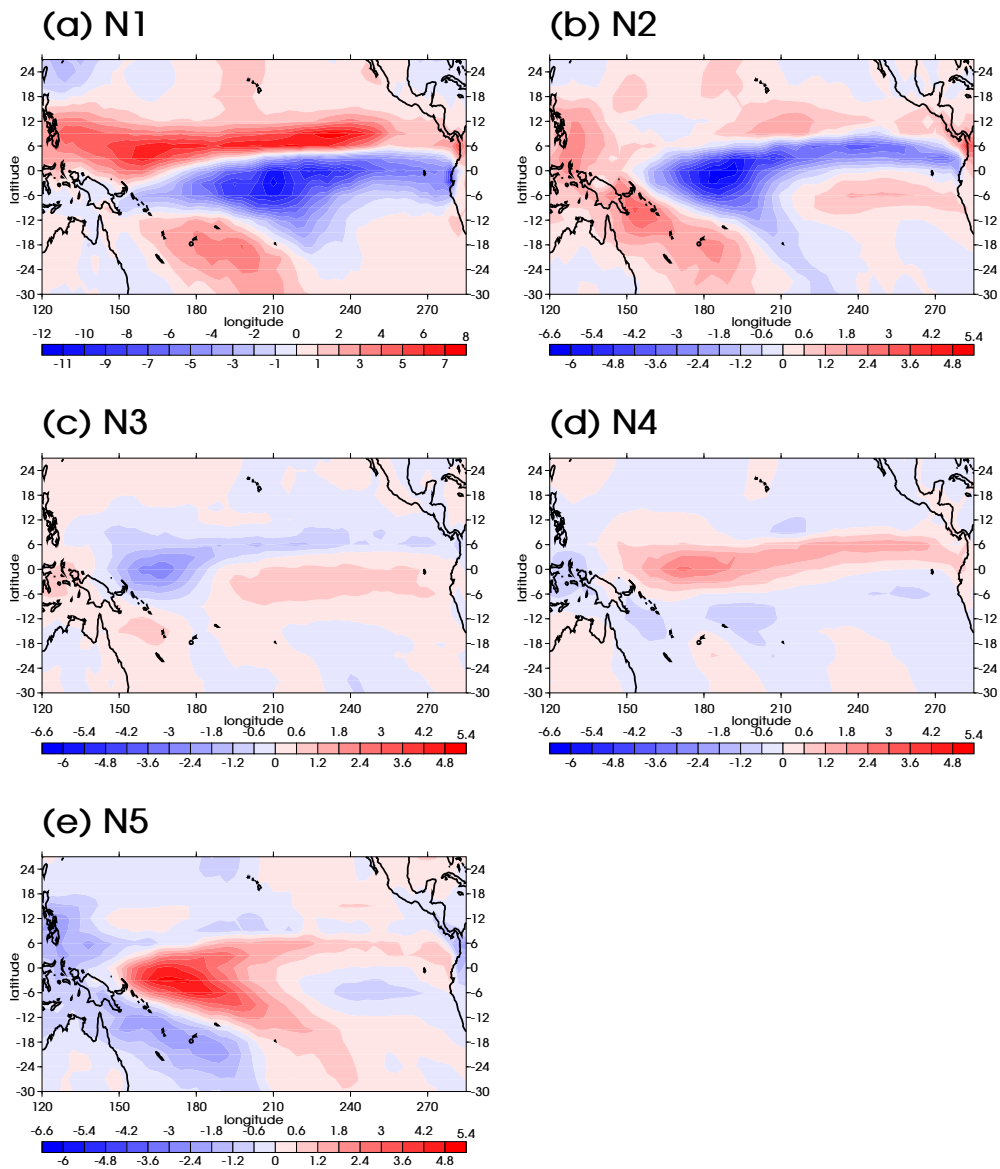


**Fig. 7** Self-Organizing Map (SOM) neurons on moisture divergence anomalies (mm/day); (a) to (e) are SOM neurons 1 to 5. Note that (a) uses a different color scale than others.

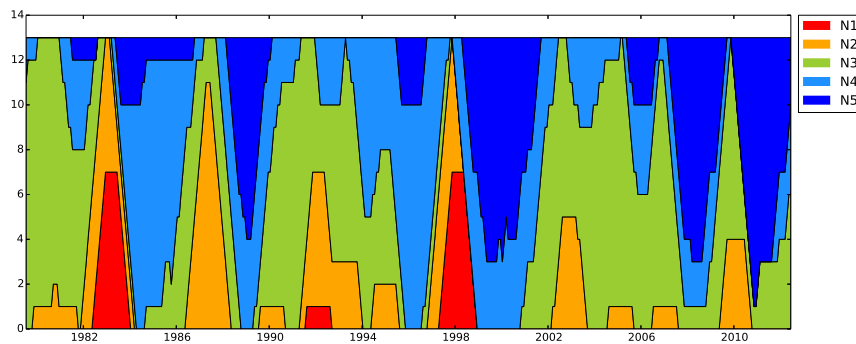


**Fig. 8** Stacked time-series of SOM training sample counts, defined as the number of training samples allocated to each neuron in each sliding 13-month time window.

tions between the neurons, thus removing the effects of magnitudes in constituting the inter-neuron distances. The moderate El Niño neuron (N2) has a much better (but opposite) pattern match with La Niña neurons (N4 and N5), than with the extreme El Niño neuron (N1). Therefore the distinction between extreme and moderate El Niños suggested by the SOM analysis is justified. On the other hand, differences between moderate El Niño and neutral (46.1 from N2 to N3) is much smaller, which is consistent with the relatively clustered data distribution in EOF #1, #2 space (Fig. 3).

#### 4 Conclusions and Discussion

We have used EOF and SOM analyses to characterize the spatial patterns of inter-annual variability in the atmospheric moisture divergence over the tropical Pacific, a key component of the hydrological cycle that is linked directly to anomalies in the surface water balance ( $E - P$ ). This variability is of course dominated by ENSO influences, with the moisture divergence shifting eastwards to follow the eastward shift of the warmest equatorial SST during moderate El Niños, accompanied by an equatorward rotation of the SPCZ. The moisture divergence anomalies associated with La Niña events have similar spatial patterns and magnitudes as moderate El Niños, but with opposite sign. Our analysis finds, however, that the moisture divergence patterns during extreme El Niño events are not simply a strengthening of the moderate El Niño pattern but exhibit distinct characteristics: the tropical convergence centre moves much further east, the NH Hadley Cell is more compact and the SPCZ swings further towards the equator. These differences from moderate El Niño behaviour are particularly apparent from the peak of the event through the decaying phase, which is consistent with previous studies using other climate variables (Kug et al, 2009; Xu and Chan, 2001).

This complex behaviour is evident in the EOF results, with a clear non-linear relationship found between the leading two PC time-series even though they are constrained by EOF analysis to have no linear dependence. This motivated our use of the SOM technique, which is not constrained by the spatial and temporal orthogonality requirements of EOF decomposition. The SOM analysis simplifies the non-linear relationship between two EOF patterns into a simple sequence of five patterns (SOM neurons) representing the range of states from La Niña to extreme El Niño. SOM neuron count time-series and inter-neuron distance/correlation statistics further validate the classification of extreme and moderate El Niños.

Our findings have a number of implications. First, a single index such as Niño 3.4 is insufficient to measure the range of atmospheric moisture divergence responses to ENSO, consistent with the prior findings for other variables (Trenberth and Stepaniak, 2001; Trenberth and Smith, 2006; Chiodi and Harrison, 2010; Kao and Yu, 2009). An index is required to represent the SST zonal contrast that distinguishes different types of El Niño, and is likely to be the key factor that causes differences in moisture divergence patterns. Our results suggest that alternatives to the conventional EOF method that are free from orthogonal constraints, such as SOM, deserve more attention when determining additional ENSO indices.

Second, analyses of ENSO behaviour need to consider more ENSO classes than the basic La Niña, neutral and El Niño classification. Our analysis of atmospheric moisture divergence demonstrates that this distinction is present in the atmospheric branch of the hydrological cycle too, providing a new perspective to the existing literature, and confirms the coupled ocean-atmosphere signature of this ENSO difference that is not necessarily implied by the SST-based analyses. The consistency with SST-based studies is not a coincidence. The sensitivity of ocean temperature and atmospheric convection is reversed between the central and eastern Pacific: central Pacific SSTAs are much more effective at inducing anomalous convection than their eastern counterpart, due to the warmer background SSTs (Kug et al, 2009; Hoerling et al, 1997; Capotondi et al, 2014), while subsurface temperature below the mixed layer has a stronger response to the thermocline changes over the eastern Pacific (Capotondi et al, 2014). Therefore once the warm SST anomalies develop over the eastern Pacific or get advected from the west in an extreme El Niño, possibly modulated by the seasonality of Kelvin wave propagation (Harrison and Schopf, 1984), or a proper timing of Australia and Asian monsoon (Xu and Chan, 2001), the induced thermocline feedback could trigger large magnitudes of deep convection over the eastern Pacific, as manifested by OLR troughs (Chiodi and Harrison, 2010), and the moisture divergence changes presented in this study for extreme El Niño (e.g. the first SOM neuron, Fig. 7a).

Similar concerns relate to the use of EOF analyses to classify ENSO behaviour – due to EOF orthogonality constraints, the pattern of variation covering La Niña to moderate El Niño events is mostly captured by EOF#1 but also partly represented in EOF#2, which in turn partly represents the contrasting moisture divergence response to moderate and extreme El Niños. Classifications need to consider this complexity and ideally use methods, such as the SOM presented here, that can rep-

resent them as separate patterns rather than the mixed form of the EOF analysis.

Third, the observed non-linear response highlights the need for a coupled Hadley-Walker cell view in explaining the different El Niño types. Although commonly interpreted as a meridional circulation cell, the Hadley cell is not zonally symmetric, but rather a 3D helix circulation where the zonal asymmetry is modulated by the Walker circulation. In neutral ENSO condition, the warm pool low and the subtropical highs to the east form a triangular shape (Fig. 5a, see also Fig.1 in Zhang and Song (2006)). In the mature phase of an extreme El Niño, strong eastern warming weakens or even reverses the Walker circulation, and compresses the equatorial-low-subtropical-high polarity (Fig. 6d); the pitch distance of the 3D Hadley-Walker helix circulation is reduced. As a result, the dry air intrusion from the subtropics becomes more effective, due to both a tighter pressure gradient and reduced opportunity for evaporation to replenish the moisture because of the shorter travel distance. The reduced trade winds and evaporation also play a role (Su and Neelin, 2002). As warming is more confined to the western-central Pacific in a moderate El Niño, the modulation of the Walker circulation is not strong enough to reverse the equatorial-low-subtropical-high polarity.

Finally, we note limitations to this study. The limited time span of ERA-I data allows only a small sample of seven El Niño events to be included. Of the three extreme El Niños, two coincided with major volcanic eruptions (the March 1982 El Chichon and the June 1991 Mt. Pinatubo), and we did not address the possible role volcanic forcing may have on tropical moisture divergence. Moreover, Pacific exhibits distinct decadal (PDO, Pacific Decadal Oscillation) to inter-decadal (IPO, Inter-decadal Pacific Oscillation) variations, with largely consistent manifestations in SST, sea level pressure, wind stress, thermocline evolution, Hadley circulation and ENSO variability (Power et al, 1999; Mantua et al, 1997; Folland and Renwick, 2002; Wang and Fiedler, 2006; Quan et al, 2004; Trenberth and Stepaniak, 2001). The change in PDO/IPO phase around 1976/77 has been identified as a major “climate shift” (Trenberth, 1990; Trenberth and Stepaniak, 2001), after which El Niño activity increased and the structure of the SPCZ changed (Folland and Renwick, 2002), possibly caused by the altered zonal SST structure (van der Wiel et al, 2015). Therefore, the validity of the results presented here might be limited to positive PDO/IPO epochs. Further investigation with earlier datasets is needed to determine whether they hold in La Niña dominated periods.

**Acknowledgements** The ERA-Interim data were extracted from ECMWF website: [http://apps.ecmwf.int/datasets/data/interim\\_full\\_daily/](http://apps.ecmwf.int/datasets/data/interim_full_daily/). The research presented in this paper was carried out on the High Performance Computing Cluster supported by the Research and Specialist Computing Support service at the University of East Anglia. Timthoy J. Osborn was supported by the Belmont Forum project SAHEWS (Natural Environment Research Council NE/L008785/1).

## 5 Appendix

### 5.1 SOM algorithms

The input moisture divergence anomaly data are organized into an  $(n \times p)$  matrix  $X$ :

$$X = \begin{bmatrix} \mathbf{x}^{(1)} \\ \mathbf{x}^{(2)} \\ \dots \\ \mathbf{x}^{(n)} \end{bmatrix} \quad (2)$$

where  $\mathbf{x}^{(i)} = (x_1^{(i)}, x_2^{(i)}, x_3^{(i)}, \dots, x_p^{(i)})$  is the  $i$ th training sample (at the  $i$ th time point).

There are several initialization options, including using random vectors/training samples or using leading EOFs (Kohonen, 2001). Different initial neurons could converge to slightly different final states, but the same overall pattern emerges at the end of training. Here, neurons were initialized by taking the first five samples from the training set  $X$ . Several SOM runs initialized with randomly chosen training samples were also performed, yielding very similar results. Therefore only results from the “first-5” initialized SOM are used here.

The initial neurons are adjusted iteratively to obtain the final neuron locations. There are two basic methods that neuron adjustments could use: incremental (or stochastic) adjustment and batch adjustment (Kohonen, 2001). In the incremental approach, neurons are adjusted using each training sample individually and in sequence. This usually leads to stochastic behaviour in the convergence path and requires large numbers of iterations to reach convergence, but is more suitable for real-time processing when a complete training set is not available beforehand. The batch mode, used here, uses all training samples together to calculate each iteration of neuron adjustment.

The training session consists of 300 iterations of neuron updates. In each iteration, each training sample is allocated to its closest neuron (in a Euclidean sense), which is called the “winner” neuron for that data sample. The training samples allocated to a particular “winner” neuron provide information on how to adjust that neuron, effectively moving its location in data space towards the weighted mean of the training samples allocated to it. However, these training samples

are also used to adjust the neurons that are neighbours of the “winner”, but subject to a weighting that depends on the topological distance between a neighbour and the “winner” neuron. This weighting is via a neighbourhood function,  $h_{ij}$ , between neurons  $i$  and  $j$  which ensures the topological relationships between neurons in the SOM. The location of each neuron  $i$  is therefore updated according to:

$$\mathbf{m}_i := \frac{\sum_j h_{ij} \bar{\mathbf{x}}_j n_j}{\sum_j h_{ij} n_j} \quad (3)$$

where the mean ( $\bar{\mathbf{x}}_j$ ) of all training samples allocated to a neighboring neuron  $\mathbf{m}_j$  is weighted by the corresponding number ( $n_j$ ) of training samples, and the neighborhood function between neurons  $i$  and  $j$ . This overall mean is then updated to  $\mathbf{m}_i$ .

A Gaussian is a common choice for the neighbourhood function, and is adopted here:

$$h_{ij}(t) = \begin{cases} \exp\left(-\frac{\|\mathbf{r}_i - \mathbf{r}_j\|^2}{2\sigma^2(t)}\right) & \sigma > 0 \\ 1 & \sigma = 0 \end{cases} \quad (4)$$

where  $\mathbf{r}_i$  and  $\mathbf{r}_j$  are the location vectors of the “winner” neuron  $i$  and the neighboring neuron  $j$ , respectively. A large kernel size,  $\sigma(t)$ , is necessary in the early stages of the training session for the global order to take shape, but this is then decreased monotonically during each iteration,  $t$ , of the training session:

$$\sigma(t) = [(\sigma_0 + 1) * (1 - \frac{t}{T})] \quad (5)$$

where  $\lfloor \cdot \rfloor$  is the floor function, and  $T$  is the total number of iterations for the training session, 300 in this case.

## 5.2 El Niño phase separation

The phase definitions for El Niños identified using the Nino 3.4 time series are shown in Fig. 9. The fast changes to Nino 3.4 and to the overlying atmosphere mean that the 70% criterion used to define the times of transition between the “Starting”, “Peak”, and “Decaying” phases do not generally occur at a calendar monthly mean value. Instead, linear interpolation between monthly mean values was used to locate the transition time points:

$$\begin{cases} f_{01} = \frac{T_2 - T_t}{T_2 - T_0} \\ f_{12} = \frac{T_t - T_0}{T_2 - T_0} \\ t_t = f_{01} \cdot t_0 + f_{12} \cdot t_2 \end{cases} \quad (6)$$

where  $T$  is the normalized Nino 3.4 index;  $t$  is the time point represented by the number of days since a

given reference time;  $f_{01}$  and  $f_{12}$  are the linear interpretation factors; subscripts 0 and 2 denote the two ends of the interpolation domain, and subscript  $t$  represents the target time/data point. Variables (e.g. moisture divergence) used to create composites for each phase were then interpolated to time point  $t$  using the same interpolation factors ( $f_{01}$  and  $f_{12}$ ).

## 6 Ethical Statement

The manuscript has not been submitted to more than one journal for simultaneous consideration, not been published previously (partly or in full). It is not split from a single study. No data have been fabricated or manipulated (including images) to support conclusions. Submission of manuscript has been approved by all co-authors, who have all contributed sufficiently to the scientific work. No human and/or animal participants are involved in the study.

## 7 Disclosure of Potential Conflict of Interest

Funding: Osborn received funding from the Belmont Forum project SAHEWS (Natural Environment Research Council NE/L008785/1).

## References

- Ashok K, Behera SK, Rao Sa, Weng H, Yamagata T (2007) El Niño Modoki and its possible teleconnection. *Journal of Geophysical Research* 112(C11):C11,007, DOI 10.1029/2006JC003798
- Bjerknes J (1966) A possible response of the atmospheric Hadley circulation to equatorial anomalies of ocean temperature. *Tellus* 4:820–829
- Bjerknes J (1969) Atmospheric teleconnections from the equatorial pacific. *Monthly Weather Review* 97(3):163–172
- Bosc C, Delcroix T (2008) Observed equatorial Rossby waves and ENSO-related warm water volume changes in the equatorial Pacific Ocean. *Journal of Geophysical Research* 113(C6):C06,003, DOI 10.1029/2007JC004613
- Bosilovich MG, Schubert S, Walker G (2005) Global changes of the water cycle intensity. *Journal of Climate* 18:1591–1608
- Cai W, Lengaigne M, Borlace S, Collins M, Cowan T, McPhaden MJ, Timmermann A, Power SB, Brown J, Menkes C, Ngari A, Vincent EM, Widlansky MJ (2012) More extreme swings of the South Pacific convergence zone due to greenhouse warming. *Nature* 488(7411):365–9, DOI 10.1038/nature11358

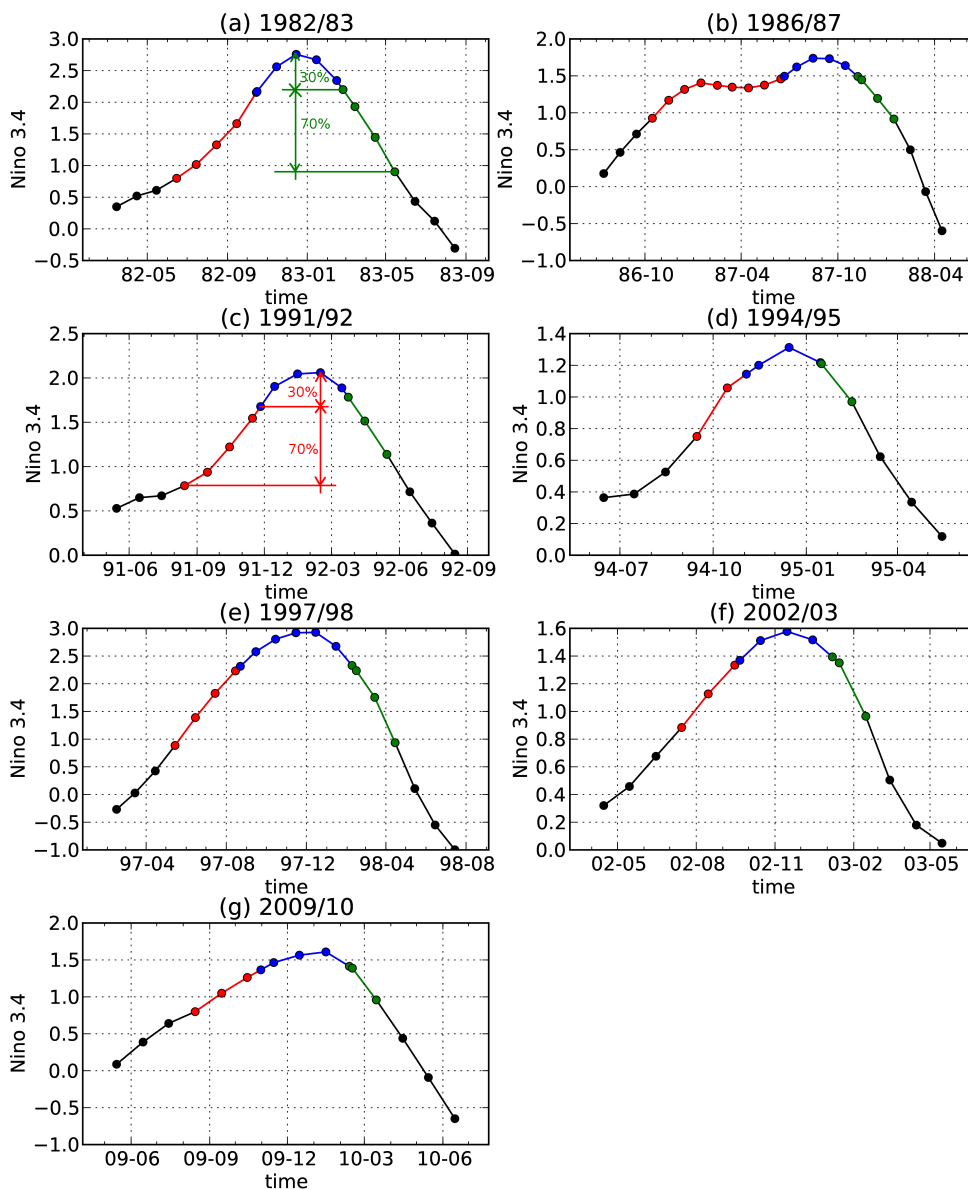


**Fig. 9** Normalized Niño 3.4 indices with phase separations for each El Niño event: (a) 1982/83, (b) 1986/87, (c) 1991/92, (d) 1994/95, (e) 1997/98, (f) 2002/03 and (g) 2009/10. Phase colors are: “Starting” (red), “Peak” (blue), “Decaying” (green), “Pre-event” and “Post-event” (both black). Panels (a) and (c) illustrate the phase separation from “Peak” to “Decaying” and from “Starting” to “Peak”, respectively.

977 Cai W, Borlace S, Lengaigne M, van Rensch P, Collins  
 978 M, Vecchi G, Timmermann A, Santoso A, McPhaden  
 979 MJ, Wu L, England MH, Wang G, Guilyardi E, Jin  
 980 FF (2014) Increasing frequency of extreme El Niño  
 981 events due to greenhouse warming. *Nature Climate*  
 982 *Change* 5(1):1–6, DOI 10.1038/nclimate2100  
 983 Capotondi A (2013) ENSO diversity in the NCAR  
 984 CCSM4 climate model. *Journal of Geophysical Re-*  
 985 *search: Oceans* 118(10):4755–4770, DOI 10.1002/  
 986 *jgrc.20335*

Capotondi A, Wittenberg AT, Newman M, Di Lorenzo  
 E, Yu JY, Braconnot P, Cole J, Dewitte B, Giese B,  
 Guilyardi E, Jin FF, Karnauskas K, Kirtman B, Lee  
 T, Schneider N, Xue Y, Yeh SW (2014) Understand-  
 ing ENSO diversity. *Bulletin of the American Meteoro-*  
 logical Society DOI 10.1175/BAMS-D-13-00117.1  
 Cavazos T (1999) Large-scale circulation anomalies  
 conducive to extreme precipitation events and deriva-  
 tion of daily rainfall in northeastern Mexico and  
 southeastern Texas. *Journal of Climate* 12:1506–1523



- 997 Chang CP, Lei Y, Sui CH, Lin X, Ren F (2012)<sup>1050</sup>  
 998 Tropical cyclone and extreme rainfall trends in East<sup>1051</sup>  
 999 Asian summer monsoon since mid-20th century. *Geo-*<sup>1052</sup>  
 1000 *physical Research Letters* 39(18):1–6, DOI 10.1029/<sup>1053</sup>  
 1001 2012GL052945 <sup>1054</sup>
- 1002 Chiodi aM, Harrison DE (2010) Characterizing warm-<sup>1055</sup>  
 1003 enso variability in the equatorial pacific: An olr<sup>1056</sup>  
 1004 perspective<sup>\*,+</sup>. *Journal of Climate* 23(9):2428–2439,<sup>1057</sup>  
 1005 DOI 10.1175/2009JCLI3030.1 <sup>1058</sup>
- 1006 Crane RG, Hewitson BC (1998) Doubled CO<sub>2</sub> precipi-<sup>1059</sup>  
 1007 tation changes for the susquehanna basin: downscal-<sup>1060</sup>  
 1008 ing from the genesis general circulation model. *Inter-*<sup>1061</sup>  
 1009 *national Journal of Climatology* 18(1):65–76 <sup>1062</sup>
- 1010 Folland C, Renwick J (2002) Relative influences of<sup>1063</sup>  
 1011 the interdecadal Pacific oscillation and ENSO on<sup>1064</sup>  
 1012 the South Pacific convergence zone. *Geophysical Re-*<sup>1065</sup>  
 1013 *search* . . . 29:2–5 <sup>1066</sup>
- 1014 Fu C, Diaz HF, Fletcher JO (1986) Characteris-<sup>1067</sup>  
 1015 tics of the Response of Sea Surface Tempera-<sup>1068</sup>  
 1016 ture in the Central Pacific Associated with Warm<sup>1069</sup>  
 1017 Episodes of the Southern Oscillation. *Monthly*<sup>1070</sup>  
 1018 *Weather Review* 114(9):1716–1739, DOI 10.1175/<sup>1071</sup>  
 1019 1520-0493(1986)114<1716:COTROS>2.0.CO;2 <sup>1072</sup>
- 1020 Galarneau TJ, Bosart LF, Schumacher RS (2010) Pre-<sup>1073</sup>  
 1021 decessor Rain Events ahead of Tropical Cyclones.<sup>1074</sup>  
 1022 *Monthly Weather Review* 138(8):3272–3297, DOI <sup>1075</sup>  
 1023 10.1175/2010MWR3243.1 <sup>1076</sup>
- 1024 Giese BS, Ray S (2011) El Niño variability in simple<sup>1077</sup>  
 1025 ocean data assimilation (SODA), 18712008. *Journal*<sup>1078</sup>  
 1026 *of Geophysical Research* 116(C2):C02,024, DOI 10.<sup>1079</sup>  
 1027 1029/2010JC006695 <sup>1080</sup>
- 1028 Gimeno L, Stohl A, Trigo RM, Dominguez F,<sup>1081</sup>  
 1029 Yoshimura K, Yu L, Drumond A, Durán-Quesada<sup>1082</sup>  
 1030 AM, Nieto R (2012) Oceanic and terrestrial sources<sup>1083</sup>  
 1031 of continental precipitation. *Reviews of Geophysics*<sup>1084</sup>  
 1032 50(4):RG4003, DOI 10.1029/2012RG000389 <sup>1085</sup>
- 1033 Harrison D, Schopf P (1984) Kelvin-wave-induced<sup>1086</sup>  
 1034 anomalous advection and the onset of surface warm-<sup>1087</sup>  
 1035 ing in El Nino events. *Monthly weather review*<sup>1088</sup>  
 1036 112:923–933 <sup>1089</sup>
- 1037 Hartmann D, KleinTank A, Rusticucci M, Alexander L,<sup>1090</sup>  
 1038 Bronnimann S, Charabi Y, Dentener F, Dlugokencky<sup>1091</sup>  
 1039 E, Easterling D, Kaplan A, Soden B, Thorne P, Wild<sup>1092</sup>  
 1040 M, Zhai P (2013) *Observations: Atmosphere and*<sup>1093</sup>  
 1041 *Surface*, Cambridge University Press, Cambridge,<sup>1094</sup>  
 1042 United Kingdom and New York, NY, USA, book sec-<sup>1095</sup>  
 1043 tion 2, p 159254. DOI 10.1017/CBO9781107415324.<sup>1096</sup>  
 1044 008 <sup>1097</sup>
- 1045 Hegerl GC, Black E, Allan RP, Ingram WJ, Polson<sup>1098</sup>  
 1046 D, Trenberth KE, Chadwick RS, Arkin PA, Saro-<sup>1099</sup>  
 1047 jini BB, Becker A, Dai A, Durack PJ, Easterling<sup>1100</sup>  
 1048 D, Fowler HJ, Kendon EJ, Huffman GJ, Liu C,<sup>1101</sup>  
 1049 Marsh R, New M, Osborn TJ, Skliris N, Stott PA,<sup>1102</sup>  
 Vidale PL, Wjffels SE, Wilcox LJ, Willett KM,  
 Zhang X (2014) Challenges in quantifying changes  
 in the global water cycle. *Bulletin of the Ameri-*  
*can Meteorological Society* p 141027152823003, DOI  
 10.1175/BAMS-D-13-00212.1
- Hewitson B, Crane R (2002) Self-organizing maps: ap-  
 plications to synoptic climatology. *Climate Research*  
 22:13–26
- Hewitson BC, Crane RG (1994) *Neural Nets: Appli-*  
*cations in Geography*. Kluwer Academic Publishers,  
 Norwell, MA, USA
- Hoerling M, Kumar A, Zhong M (1997) El Niño, La  
 Niña, and the nonlinearity of their teleconnections.  
*Journal of Climate* 10:1769–1786
- Hu Y, Fu Q (2007) Observed poleward expansion of the  
 Hadley circulation since 1979. *Atmospheric Chem-*  
*istry and Physics* 7(19):5229–5236, DOI 10.5194/  
 acp-7-5229-2007
- Johnson NC (2013) How Many ENSO Flavors Can We  
 Distinguish?\*. *Journal of Climate* 26(13):4816–4827,  
 DOI 10.1175/JCLI-D-12-00649.1
- Kalnay E, Kanamitsu M, Kistler R, Collins W, Deaven  
 D, Gandin L, Iredell M, Saha S, White G, Woollen  
 J, Zhu Y, Chelliah M, Ebisuzaki W, Higgins W,  
 Janowiak J, Mo K, Ropelewski C, Wang J, Leet-  
 maa A, Reynolds R, Jenne R, Joseph D (1996) The  
 NCEP/NCAR 40-Year Reanalysis Project. *Bulletin*  
*of the American Meteorological Society* 77(3):437–  
 471
- Kao HY, Yu JY (2009) Contrasting Eastern-Pacific and  
 Central-Pacific Types of ENSO. *Journal of Climate*  
 22(3):615–632, DOI 10.1175/2008JCLI2309.1
- Kistler R, Kalnay E, Collins W, Saha S, White G,  
 Woollen J, Chelliah M, Ebisuzaki W, Kanamitsu  
 M, Kousky V, van den Dool H, Jenne R, Fior-  
 ino M (2001) The NCEP-NCAR 50-year reanalysis:  
 Monthly means CD-ROM and documentation. *Bul-*  
*letin of the American Meteorological Society* *Ameri-*  
*can* 82:247–268
- Knippertz P, Wernli H (2010) A Lagrangian Clima-  
 tology of Tropical Moisture Exports to the North-  
 ern Hemispheric Extratropics. *Journal of Climate*  
 23(4):987–1003, DOI 10.1175/2009JCLI3333.1
- Knippertz P, Wernli H, Gläser G (2013) A Global  
 Climatology of Tropical Moisture Exports. *Jour-*  
*nal of Climate* 26(10):3031–3045, DOI 10.1175/  
 JCLI-D-12-00401.1
- Kohonen T (1990) The self-organizing map. *Proceed-*  
*ings of the IEEE* 78(9):1464–1480
- Kohonen T (2001) *Self-Organizing Maps*. Physics and  
 astronomy online library, Springer Berlin Heidelberg
- Kug JS, Jin FF, An SI (2009) Two Types of El Niño  
 Events: Cold Tongue El Niño and Warm Pool El

- Niño. *Journal of Climate* 22(6):1499–1515, DOI 10.1175/2008JCLI2624.1
- Larkin NK, Harrison DE (2005a) Global seasonal temperature and precipitation anomalies during El Niño autumn and winter. *Geophysical Research Letters* 32(16):L16,705, DOI 10.1029/2005GL022860
- Larkin NK, Harrison DE (2005b) On the definition of El Niño and associated seasonal average U.S. weather anomalies. *Geophysical Research Letters* 32(13):L13,705, DOI 10.1029/2005GL022738
- Liu Y, Weisberg RH, Mooers CNK (2006) Performance evaluation of the self-organizing map for feature extraction. *Journal of Geophysical Research* 111(C5):C05,018, DOI 10.1029/2005JC003117
- Lorenz C, Kunstmann H (2012) The Hydrological Cycle in Three State-of-the-Art Reanalyses: Intercomparison and Performance Analysis. *Journal of Hydrometeorology* 13(5):1397–1420, DOI 10.1175/JHM-D-11-088.1
- Mantua NJ, Hare SR, Zhang Y, Wallace JM, Francis RC (1997) A Pacific Interdecadal Climate Oscillation with Impacts on Salmon Production. *Bulletin of the American Meteorological Society* 78(6):1069–1079, DOI 10.1175/1520-0477(1997)078<1069:APICOW>2.0.CO;2
- Mo K, Higgins R (1996) Large-scale atmospheric moisture transport as evaluated in the NCEP/NCAR and the NASA/DAO reanalyses. *Journal of Climate* 9:1531–1545
- Oort AH, Yienger JJ (1996) Observed Interannual Variability in the Hadley Circulation and Its Connection to ENSO. *Journal of Climate* 9(11):2751–2767, DOI 10.1175/1520-0442(1996)009<2751:OIVITH>2.0.CO;2
- Pan M, Sahoo AK, Troy TJ, Vinukollu RK, Sheffield J, Wood EF (2012) Multisource Estimation of Long-Term Terrestrial Water Budget for Major Global River Basins. *Journal of Climate* 25(9):3191–3206, DOI 10.1175/JCLI-D-11-00300.1
- Power S, Casey T, Folland C, Colman a, Mehta V (1999) Inter-decadal modulation of the impact of ENSO on Australia. *Climate Dynamics* 15(5):319–324, DOI 10.1007/s003820050284
- Praveen Kumar B, Vialard J, Lengaigne M, Murty VSN, McPhaden MJ (2011) TropFlux: air-sea fluxes for the global tropical oceans description and evaluation. *Climate Dynamics* 38(7-8):1521–1543, DOI 10.1007/s00382-011-1115-0
- Quan Xw, Diaz HF, Hoerling MP (2004) Change in the tropical Hadley cell since 1950. In: Diaz H, Bradley R (eds) *The Hadley Circulation: Past, Present, and Future*, Kluwer Academic Publishers, Dordrecht, pp 85–120
- Reusch DB, Alley RB, Hewitson BC (2007) North Atlantic climate variability from a self-organizing map perspective. *Journal of Geophysical Research* 112(D2):1–20, DOI 10.1029/2006JD007460
- Roads J (2002) Closing the water cycle. *GEWEX Newsletter* 12(1):6–8
- Roads J (2003) The NCEP-NCAR, NCEP-DOE, and TRMM tropical atmosphere hydrologic cycles. *Journal of Hydrometeorology* 4:826–840
- Robertson FR, Bosilovich MG, Chen J, Miller TL (2011) The Effect of Satellite Observing System Changes on MERRA Water and Energy Fluxes. *Journal of Climate* 24(20):5197–5217, DOI 10.1175/2011JCLI4227.1
- Rodríguez JM, Johns TC, Thorpe RB, Wiltshire a (2010) Using moisture conservation to evaluate oceanic surface freshwater fluxes in climate models. *Climate Dynamics* 37(1-2):205–219, DOI 10.1007/s00382-010-0899-7
- Singh A, Delcroix T, Cravatte S (2011) Contrasting the flavors of El Niño-Southern Oscillation using sea surface salinity observations. *Journal of Geophysical Research* 116(C6):C06,016, DOI 10.1029/2010JC006862
- Soden BJ (2000) The sensitivity of the tropical hydrological cycle to ENSO. *Journal of Climate* 13:538–550
- Su H, Neelin J (2002) Teleconnection Mechanisms for Tropical Pacific Descent Anomalies during El Niño\*. *Journal of the atmospheric sciences* 59:2694–2712
- Trenberth KE (1990) Recent Observed Interdecadal Climate Changes in the Northern Hemisphere. *Bulletin of the American Meteorological Society* 71(7):988–993, DOI 10.1175/1520-0477(1990)071<0988:ROICCI>2.0.CO;2
- Trenberth KE (1997a) The Definition of El Niño. *Bulletin of the American Meteorological Society* 78(August):2771–2777
- Trenberth KE (1997b) Using Atmospheric Budgets as a Constraint on Surface Fluxes. *Journal of Climate* 10(11):2796–2809, DOI 10.1175/1520-0442(1997)010<2796:UABAAC>2.0.CO;2
- Trenberth KE, Guillemot CJ (1998) Evaluation of the atmospheric moisture and hydrological cycle in the NCEP/NCAR reanalyses. *Climate Dynamics* 14(3):213–231, DOI 10.1007/s003820050219
- Trenberth KE, Smith L (2006) The vertical structure of temperature in the tropics: Different flavors of El Niño. *Journal of climate* 19(2005):4956–4970
- Trenberth KE, Stepaniak DP (2001) Indices of El Niño Evolution. *Journal of Climate* 14(8):1697–1701, DOI 10.1175/1520-0442(2001)014<1697:LIOENO>2.0.CO;2
- Trenberth KE, Dai A, Rasmussen RM, Parsons DB (2003) The Changing Character of Precipitation.

- 1209 Bulletin of the American Meteorological Society<sup>1262</sup> the tropical Pacific. *Geophysical Research Letters*  
1210 84(9):1205–1217, DOI 10.1175/BAMS-84-9-1205 <sup>1263</sup> 33(12):L12,701, DOI 10.1029/2006GL025942
- 1211 Trenberth KE, Smith L, Qian T, Dai A, Fasullo JT  
1212 (2007) Estimates of the Global Water Budget and Its  
1213 Annual Cycle Using Observational and Model Data.  
1214 *Journal of Hydrometeorology* 8(4):758–769, DOI 10.  
1215 1175/JHM600.1
- 1216 Trenberth KE, Fasullo JT, Mackaro J (2011) Atmo-  
1217 spheric Moisture Transports from Ocean to Land and  
1218 Global Energy Flows in Reanalyses. *Journal of Cli-  
1219 mate* 24(18):4907–4924, DOI 10.1175/2011JCLI4171.  
1220 1
- 1221 Verdon-Kidd DC, Kiem AS (2009) On the relationship  
1222 between large-scale climate modes and regional syn-  
1223 optic patterns that drive Victorian rainfall. *Hydrol-  
1224 ogy and Earth System Sciences* 13(4):467–479, DOI  
1225 10.5194/hess-13-467-2009
- 1226 Verdon-Kidd DC, Kiem aS, Moran R (2014) Links  
1227 between the big dry in Australia and hemispheric  
1228 multi-decadal climate variability-implications for wa-  
1229 ter resource management. *Hydrology and Earth  
1230 System Sciences* 18(6):2235–2256, DOI 10.5194/  
1231 hess-18-2235-2014
- 1232 Wang C (2002) Atmospheric Circulation Cells As-  
1233 sociated with the El NiñoSouthern Oscillation.  
1234 *Journal of Climate* 15(4):399–419, DOI 10.1175/  
1235 1520-0442(2002)015<0399:ACCAWT>2.0.CO;2
- 1236 Wang C, Fiedler PC (2006) ENSO variability and  
1237 the eastern tropical Pacific: A review. *Progress  
1238 in Oceanography* 69(2-4):239–266, DOI 10.1016/j.  
1239 pocean.2006.03.004
- 1240 Wang K, Dickinson RE (2012) A review of global terres-  
1241 trial evapotranspiration: Observation, modeling, cli-  
1242 matology, and climatic variability. *Reviews of Geo-  
1243 physics* 50(2):1–54, DOI 10.1029/2011RG000373
- 1244 van der Wiel K, Matthews AJ, Stevens DP, Joshi MM  
1245 (2015) A dynamical framework for the origin of the  
1246 diagonal south pacific and south atlantic convergence  
1247 zones. *Quarterly Journal of the Royal Meteorological  
1248 Society* pp n/a–n/a, DOI 10.1002/qj.2508
- 1249 Xu J, Chan J (2001) The role of the Asian-Australian  
1250 monsoon system in the onset time of El Niño events.  
1251 *Journal of climate* 14:418–433
- 1252 Yu JY, Kao HY (2007) Decadal changes of ENSO  
1253 persistence barrier in SST and ocean heat content  
1254 indices: 19582001. *Journal of Geophysical Research*  
1255 112(D13):D13,106, DOI 10.1029/2006JD007654
- 1256 Zahn M, Allan RP (2011) Changes in water vapor  
1257 transports of the ascending branch of the tropi-  
1258 cal circulation. *Journal of Geophysical Research*  
1259 116(D18):D18,111, DOI 10.1029/2011JD016206
- 1260 Zhang M, Song H (2006) Evidence of deceleration  
1261 of atmospheric vertical overturning circulation over